

A Favre-Averaged Shallow Water Framework for Aerated Flows with Friction Factor Decomposition

Matthias Kramer

School of Engineering and Technology (SET)

The University of New South Wales, Canberra, Australia

m.kramer@unsw.edu.au

January 2026

Abstract

Accurate prediction of flow resistance in high-Froude-number aerated flows remains challenging due to air entrainment, which causes strong spatial variability in mixture density. In this work, we introduce a density-weighted (Favre) averaging approach to rigorously account for vertical distributions of air concentration and velocity. Favre averaging naturally captures variations in mixture density induced by air entrainment, thereby enabling a density-consistent Shallow Water Equation (SWE) formulation for aerated flows. Within this framework, we present a novel Darcy–Weisbach friction factor formulation that decomposes contributions associated with uniform flow, spatially varying flow, and temporally evolving flow, and incorporates momentum and pressure correction factors reflecting the vertical structure of the mixture. Application to experimental data from the literature demonstrates that the Favre-averaged SWE framework provides a physically consistent means of quantifying effective friction. Overall, this work establishes a mechanistic, density-weighted methodology for modelling resistance in high-Froude-number aerated flows, provides new physical insight into the role of aeration in frictional dissipation, and lays a rational foundation for future modelling of unsteady and rapidly varied aerated flows.

Keywords: shallow water, aerated flows, Favre averaging, friction factor

1 Introduction

High-Froude-number, boundary-layer-type open-channel flows often exhibit self-aeration due to strong turbulence and surface instabilities. The entrainment of air modifies the mixture density, turbulence structure, and momentum distribution, which strongly influence hydraulic resistance, energy dissipation, and flow dynamics. Accurately predicting friction in these flows is essential for a wide range of environmental and engineering applications, from river hydraulics to industrial water transport.

In the aerated flow literature, the most commonly used friction factor formulation is of Darcy–Weisbach type (Wood, 1991; Chanson, 1992; Boes, 2000; Ruff & Ward, 2002; Chanson, 2004)

$$f_e = \frac{8gd_{\text{eq}}S_f}{\langle u_w \rangle^2} = \frac{8gd_{\text{eq}}^3S_f}{q^2}, \quad (1)$$

where $\langle \overline{u_w} \rangle$ is the mean water velocity, averaged over both flow depth and time, g is the acceleration due to gravity, $q = \langle \overline{u_w} \rangle d_{\text{eq}}$ is the specific water flow rate, $S_f = \tau_0/(\rho_w g d_{\text{eq}})$ is the friction slope with τ_0 the bed shear stress and ρ_w the water density, and d_{eq} is the equivalent clear-water depth, defined as

$$d_{\text{eq}} = \int_{z=0}^{z_0} (1 - \bar{c}) \, dz \quad (2)$$

where \bar{c} is the time-averaged volumetric air concentration, z is the bed-normal coordinate, measured positive upward from the channel bed, and z_0 denotes the mixture flow depth where $\bar{c} = 0.9$. Here, the operators $\langle \cdot \rangle$ and $\langle \cdot \rangle$ indicate time and spatial averaging, respectively. Equation (1) is derived from control volume momentum considerations, where the bed shear stress balances the streamwise momentum loss. In this formulation, the friction slope S_f can alternatively be expressed from an energy perspective, as the head loss per unit length

$$S_f = S_0 - \frac{\partial H_m}{\partial x}, \quad (3)$$

where H_m is the mean total head of the mixture referenced to the channel bed elevation z_0 , measured vertically from a fixed datum, x is the streamwise coordinate along the channel bed, and $S_0 = -\partial z_0 / \partial x$ is the bed slope. For steady, uniform flow conditions, the friction slope equals the bed slope, i.e., $S_f = S_0$.

Despite its widespread use, (1) presents several important limitations. First, it has mostly been applied for uniform flow (Chanson, 1992, 1993; Boes & Hager, 2003; Bung, 2009; Wang *et al.*, 2022), and where non-uniform flows are considered, correction factors accounting for non-uniform velocity distributions are often neglected (Felder & Chanson, 2011; Scheres *et al.*, 2020; Mozer *et al.*, 2025). Second, pressure correction factors, which account for the effects of the air–water mixture on the flow, are mostly absent from literature formulations. Third, (1) is restricted to steady conditions and does not account for temporal variations of depth or velocity, which may be significant in transient aerated flows.

Thus, there is a clear need for a unifying friction framework that is rigorously derived and accounts for both spatial and temporal variations in aerated flows.

In this study, we address this critical gap by deriving a Darcy–Weisbach friction factor formulation within a density-weighted Shallow Water Equation (SWE) framework. We first introduce a Favre averaging approach for aerated flows (§ 2.1), which is then applied to derive the corresponding Favre- and depth-averaged mixture continuity and momentum equations (§ 2.2). Building on this framework, we present a decomposition of the friction factor that explicitly separates contributions from uniform flow, spatially varying flow, and temporally evolving flow (§ 2.3). The formulation further incorporates momentum and pressure correction factors to account for the vertical distribution of air, providing a mechanistic, physically consistent approach for predicting effective friction in aerated high-Froude-number flows. The applicability of the proposed approach is demonstrated using an existing experimental dataset (§ 3), followed by a discussion (§ 4) in which limitations and the broader implications of the developed framework are highlighted.

2 Methods

Below, we introduce density-weighted (Favre) averaging for aerated mixtures and define the key quantities and correction factors required to describe the non-uniform vertical structure of the flow. These definitions form the basis for the subsequent derivation of the Favre- and depth-averaged continuity and momentum equations.

2.1 Favre averaging in aerated flows

In aerated flows, the local mixture density can vary significantly due to entrained air. To properly account for the effects of density fluctuations and to preserve conservation of mass and momentum, it is useful to employ Favre averages.

2.1.1 Definition of Favre averages

For an arbitrary quantity ϕ , the Favre average is defined as (Favre, 1965, 1969)

$$\tilde{\phi} = \overline{\frac{\rho_m \phi}{\rho_m}}, \quad \phi = \tilde{\phi} + \phi'', \quad (4)$$

where ρ_m is the instantaneous mixture density, the operator $(\tilde{\cdot})$ denotes Favre-averaging, and ϕ'' is the Favre fluctuation, which satisfies by construction

$$\overline{\rho_m \phi''} = 0. \quad (5)$$

For aerated open-channel flows, the time-average of the mixture density multiplied by a quantity ϕ can be expressed as

$$\overline{\rho_m \phi} = \rho_a \overline{c \phi} + \rho_w \overline{(1-c) \phi} \approx \rho_w \overline{(1-c) \phi}, \quad (6)$$

where c is the instantaneous volumetric air concentration, ρ_a and ρ_w are the densities of air and water, respectively. Since $\rho_a \ll \rho_w$, the term $\rho_a \overline{c \phi}$ is neglected.

Depth-averaged Favre quantities are obtained by integrating from the channel bed ($z = 0$) to the characteristic mixture depth z_{90} , following Wood (1991). Droplet flow above z_{90} is neglected as it contributes negligibly to mass and momentum transport (Chanson, 1995, 1997). Combining Favre averaging with the density approximation $\overline{\rho_m} \approx \rho_w (1 - \bar{c})$ yields a Favre- and depth-averaged quantity

$$\langle \tilde{\phi} \rangle = \frac{\int_{z=0}^{z_{90}} \overline{\rho_m \phi} dz}{\int_{z=0}^{z_{90}} \overline{\rho_m} dz} \approx \frac{\rho_w \int_{z=0}^{z_{90}} (1 - \bar{c}) \overline{\phi} dz}{\rho_w \int_{z=0}^{z_{90}} (1 - \bar{c}) dz} = \frac{\int_{z=0}^{z_{90}} (1 - \bar{c}) \overline{\phi} dz}{d_{eq}}, \quad (7)$$

where the equivalent clear-water depth appears in the denominator. Equation (7) assumes that fluctuations of c are weakly correlated with ϕ , which is reasonable for bulk aerated flows. Key Favre-averaged quantities used later in the development of the shallow water framework are:

- Mixture mass ($\phi = 1$)

$$\langle \tilde{1} \rangle = \frac{\int_{z=0}^{z_{90}} \overline{\rho_m} dz}{\int_{z=0}^{z_{90}} \overline{\rho_m} dz} \approx \frac{\int_{z=0}^{z_{90}} (1 - \bar{c}) dz}{d_{eq}} = 1, \quad (8)$$

- Mixture velocity ($\phi = u_m$)

$$\langle \tilde{u_m} \rangle = \frac{\int_{z=0}^{z_{90}} \overline{\rho_m u_m} dz}{\int_{z=0}^{z_{90}} \overline{\rho_m} dz} \approx \frac{\int_{z=0}^{z_{90}} (1 - \bar{c}) \overline{u_m} dz}{d_{eq}}, \quad (9)$$

- Squared velocity ($\phi = u_m^2$)

$$\langle \tilde{u_m^2} \rangle = \frac{\int_{z=0}^{z_{90}} \overline{\rho_m u_m^2} dz}{\int_{z=0}^{z_{90}} \overline{\rho_m} dz} \approx \frac{\int_{z=0}^{z_{90}} (1 - \bar{c}) \overline{u_m^2} dz}{d_{eq}}. \quad (10)$$

It is important to note that the Favre- and depth-averaged mixture velocity $\langle \tilde{u_m} \rangle$ corresponds to the mean water velocity, i.e., $\langle \tilde{u_m} \rangle \approx \langle \overline{u_w} \rangle$, which naturally follows from the density weighting approach. In the context of $\langle \tilde{u_m^2} \rangle$, the momentum correction factor β , which accounts for the vertical non-uniformity of the velocity and mixture density, is then

$$\beta = \frac{\langle \tilde{u_m^2} \rangle}{\langle \tilde{u_m} \rangle^2} = \frac{\int_{z=0}^{z_{90}} (1 - \bar{c}) \overline{u_m^2} dz}{d_{eq} \langle \tilde{u_m} \rangle^2}. \quad (11)$$

2.1.2 Depth-integrated pressure and Favre centroid

Under the hydrostatic assumption, the vertical momentum balance reads

$$\frac{\partial \overline{p_m}}{\partial z} = -\overline{\rho_m} g \cos \theta, \quad (12)$$

where $\overline{p_m}$ is the mixture pressure and $\theta = \arcsin(S_0)$ is the bed slope angle. Approximating the mixture density as $\overline{\rho_m} \approx \rho_w(1 - \bar{c})$ and integrating from z to the mixture depth z_{90} , where $\overline{p_m}(z_{90}) = 0$, gives

$$\overline{p_m}(z) = \rho_w g \cos \theta \int_{z=0}^{z_{90}} (1 - \bar{c}(\zeta)) d\zeta, \quad (13)$$

where ζ is a dummy variable. The depth-integrated pressure force per unit width, which appears in the depth-averaged momentum equation, is

$$\int_{z=0}^{z_{90}} \overline{p_m} dz = \rho_w g \cos \theta \int_{z=0}^{z_{90}} \left[\int_z^{z_{90}} (1 - \bar{c}(\zeta)) d\zeta \right] dz. \quad (14)$$

Introducing the Favre centroid of the mixture

$$\langle \tilde{z} \rangle = \frac{\int_{z=0}^{z_{90}} (1 - \bar{c}) z dz}{d_{\text{eq}}}, \quad (15)$$

the depth-integrated pressure can be written compactly as

$$\int_{z=0}^{z_{90}} \overline{p_m} dz = \rho_w g \cos \theta d_{\text{eq}} \langle \tilde{z} \rangle. \quad (16)$$

To make the analogy with the classical hydrostatic term $\frac{1}{2} \rho_w g \cos \theta d_{\text{eq}}^2$, we define the pressure correction factor Ω as

$$\Omega = \frac{2\langle \tilde{z} \rangle}{d_{\text{eq}}} = \frac{\int_{z=0}^{z_{90}} (1 - \bar{c}) z dz}{\frac{1}{2} d_{\text{eq}}^2}, \quad (17)$$

so that the depth-integrated pressure can also be written in the familiar form

$$\int_{z=0}^{z_{90}} \overline{p_m} dz = \frac{1}{2} \rho_w g \cos \theta \Omega d_{\text{eq}}^2. \quad (18)$$

2.2 Density-weighted shallow-water framework for aerated flows

2.2.1 Mixture continuity equation

Aerated open-channel flows are gravity-driven flows over solid boundaries, where friction opposes the motion induced by gravity. Assuming that the flow is predominantly two-dimensional, the local Favre-averaged continuity equation is expressed as (Wilcox, 1993; Gatski & Bonnet, 2009)

$$\frac{\partial \overline{\rho_m}}{\partial t} + \frac{\partial}{\partial x} (\overline{\rho_m} \tilde{u}_m) + \frac{\partial}{\partial z} (\overline{\rho_m} \tilde{w}_m) = 0, \quad (19)$$

with \tilde{u}_m and \tilde{w}_m are the Favre-averaged mixture velocities in the streamwise and vertical directions, respectively. Integrating (19) from the channel bed ($z = 0$) to the characteristic mixture depth z_{90} , and applying the Leibniz rule together with the free-surface kinematic boundary condition $\tilde{w}_m(z_{90}) = \partial z_{90}/\partial t + \tilde{u}_m(z_{90}) \partial z_{90}/\partial x$, yields

$$\frac{\partial}{\partial t} \int_{z=0}^{z_0} \overline{\rho_m} dz + \frac{\partial}{\partial x} \int_{z=0}^{z_0} \overline{\rho_m} \tilde{u}_m dz = 0. \quad (20)$$

Using depth-averaged Favre quantities defined in (8) and (9), the depth-integrated mixture mass and momentum are approximated as

$$\int_{z=0}^{z_0} \overline{\rho_m} dz \approx \rho_w d_{\text{eq}}, \quad (21)$$

$$\int_{z=0}^{z_0} \overline{\rho_m} \tilde{u}_m dz \approx \rho_w d_{\text{eq}} \langle \tilde{u}_m \rangle. \quad (22)$$

Substituting (21) and (22) into (20) and dividing by ρ_w gives

$$\frac{\partial d_{\text{eq}}}{\partial t} + \langle \tilde{u}_m \rangle \frac{\partial d_{\text{eq}}}{\partial x} + d_{\text{eq}} \frac{\partial \langle \tilde{u}_m \rangle}{\partial x} = 0, \quad (23)$$

where the derivative $\partial(d_{\text{eq}} \langle \tilde{u}_m \rangle) / \partial x$ has been expanded. Equation (23) describes depth-averaged mass conservation for flows with spatial and temporal variability and forms a key component of the density-weighted shallow water framework for aerated flows.

2.2.2 Streamwise mixture momentum equation

The two-dimensional streamwise component of the Favre-averaged mixture equation reads (Wilcox, 1993; Gatski & Bonnet, 2009)

$$\begin{aligned} & \frac{\partial}{\partial t} (\overline{\rho_m} \tilde{u}_m) + \frac{\partial}{\partial x} (\overline{\rho_m} \tilde{u}_m^2) + \frac{\partial}{\partial z} (\overline{\rho_m} \tilde{u}_m \tilde{w}_m) \\ &= \overline{\rho_m} g_x - \frac{\partial \overline{p_m}}{\partial x} + \frac{\partial \overline{\tau_{xx}}}{\partial x} + \frac{\partial \overline{\tau_{xz}}}{\partial z} - \frac{\partial}{\partial x} \left(\overline{\rho_m u''_m^2} \right) - \frac{\partial}{\partial z} \left(\overline{\rho_m u''_m w''_m} \right), \end{aligned} \quad (24)$$

where τ_{xx} and τ_{xz} are the viscous normal and shear stresses, $g_x = g S_0$ is the streamwise component of gravitational acceleration associated with the bed slope, and u''_m , w''_m are the streamwise and vertical Favre velocity fluctuations, respectively. Integrating (24) over the flow depth $z \in [0, z_0]$ and applying the Leibniz rule, together with the bed boundary condition $\tilde{w}_m(0) = 0$ and the free-surface kinematic condition, yields the depth-integrated momentum balance

$$\frac{\partial}{\partial t} \int_{z=0}^{z_0} \overline{\rho_m} \tilde{u}_m dz + \frac{\partial}{\partial x} \int_{z=0}^{z_0} \overline{\rho_m} \tilde{u}_m^2 dz = \int_{z=0}^{z_0} \overline{\rho_m} g_x dz - \frac{\partial}{\partial x} \int_{z=0}^{z_0} \overline{p_m} dz - \tau_0, \quad (25)$$

where the bed shear stress τ_0 arises from vertical viscous and turbulent fluxes

$$\tau_0 = - \int_{z=0}^{z_0} \frac{\partial}{\partial z} \left(\tau_{xz} - \overline{\rho_m u''_m w''_m} \right) dz. \quad (26)$$

Note that streamwise viscous and turbulent stress gradients are neglected in the depth-integrated equation, as their contributions are small compared to the corresponding vertical fluxes in shallow, high-Froude-number, gravity-driven flows, consistent with classical shallow-water formulations.

The depth-integrated mixture momentum and the mixture momentum flux are closed using Favre-averaged quantities defined in (9) and (10), while the depth-integrated pressure is evaluated using (16). Accordingly,

$$\int_{z=0}^{z_0} \overline{\rho_m} \tilde{u}_m dz \approx \rho_w d_{\text{eq}} \langle \tilde{u}_m \rangle, \quad (27)$$

$$\int_{z=0}^{z=90} \overline{\rho_m} \tilde{u_m}^2 dz \approx \rho_w d_{\text{eq}} \beta \langle \tilde{u_m} \rangle^2, \quad (28)$$

and, assuming hydrostatic conditions,

$$\int_{z=0}^{z=90} \overline{p_m} dz \approx \frac{1}{2} \rho_w g \cos \theta \Omega d_{\text{eq}}^2, \quad (29)$$

where β and Ω are the momentum and pressure correction factors defined in (11) and (17), respectively. Similar air–water correction factors have been proposed previously (Ohtsu *et al.*, 2004; Chanson & Aroquipa Nina, 2024), and their relationship to the present analysis is discussed in § 3.1.

The depth-integrated gravitational forcing term is evaluated using the approximation $\overline{\rho_m} \approx \rho_w (1 - \bar{c})$, which yields

$$\int_{z=0}^{z=90} \overline{\rho_m} g_x dz \approx \rho_w \int_{z=0}^{z=90} (1 - \bar{c}) g S_0 dz = \rho_w g d_{\text{eq}} S_0. \quad (30)$$

Combining (25) with (27) to (30) and dividing by ρ_w , leads to the depth-averaged streamwise momentum equation of the density-weighted shallow water framework for aerated flows

$$\frac{\partial (d_{\text{eq}} \langle \tilde{u_m} \rangle)}{\partial t} + \frac{\partial (\beta d_{\text{eq}} \langle \tilde{u_m} \rangle^2)}{\partial x} = g d_{\text{eq}} S_0 - \frac{\partial}{\partial x} \left(\frac{1}{2} g \Omega d_{\text{eq}}^2 \cos \theta \right) - \frac{\tau_0}{\rho_w}. \quad (31)$$

2.3 Effective friction factor formulation

2.3.1 General decomposition of the effective friction factor

To derive an explicit expression for the friction factor, closure of the depth-averaged momentum equation requires a representation of the bed shear stress. For aerated open-channel flows, the bed shear stress is expressed in Darcy–Weisbach form as

$$\tau_0 = \frac{1}{8} \rho_w f_e \langle \tilde{u_m} \rangle^2, \quad (32)$$

where f_e is the effective friction factor of the aerated flow and $\langle \tilde{u_m} \rangle$ is the Favre-averaged mixture velocity. Substituting this expression into (31), and performing the algebraic manipulations outlined in Appendix A yields the explicit decomposition

$$f_e = \underbrace{\frac{8 g d_{\text{eq}} S_0}{\langle \tilde{u_m} \rangle^2}}_{\text{uniform flow}} + \underbrace{\frac{8}{\langle \tilde{u_m} \rangle^2} \left(-\frac{\Delta \left(\frac{1}{2} g \Omega d_{\text{eq}}^2 \cos \theta \right)}{\Delta x} - \frac{\Delta (\beta d_{\text{eq}} \langle \tilde{u_m} \rangle^2)}{\Delta x} \right)}_{\text{spatially varying flow}} + \underbrace{\frac{8}{\langle \tilde{u_m} \rangle^2} \left(-\frac{\Delta (d_{\text{eq}} \langle \tilde{u_m} \rangle)}{\Delta t} \right)}_{\text{temporally varying flow}}, \quad (33)$$

where spatial and temporal derivatives are expressed as finite differences, allowing direct evaluation from measured or simulated depth and velocity profiles. Equation (33) shows that f_e is an effective quantity incorporating flow development and aeration-induced pressure effects. The first term recovers the classical Darcy–Weisbach expression for uniform, steady flow, while the second and third terms represent spatial and

temporal departures from uniformity, respectively, modified by the pressure and momentum correction factors Ω and β .

For steady, spatially developing flows, the temporal term vanishes. Further assuming gradual spatial variations in β and Ω , the friction factor reduces to the Gradually Varied Flow (GVF) form (Appendix A)

$$f_e = \frac{8}{Fr^2} \left(S_0 + \frac{\Delta d_{eq}}{\Delta x} \left(\beta Fr^2 - \Omega \cos \theta \right) \right), \quad (34)$$

with the Froude number defined as $Fr = \langle \tilde{u}_m \rangle / \sqrt{g d_{eq}}$. Equation (34) provides a practical and explicit expression for the friction factor in steadily developing, gradually varied aerated flows, while retaining corrections associated with aeration and non-uniform velocity profiles.

An alternative GVF friction factor formulation can be derived from energy considerations, yielding an expression identical to the momentum-based formulation (Appendix B). In this energy-based approach, the correction factors in (34) are replaced by the kinetic energy correction factor α and the energy-based pressure correction factor Ω_E , which include an additional Favre-averaged velocity term (see Appendix B). As a general rule, the energy-based formulation should be used when quantities related to energy fluxes are of interest, such as energy dissipation or head losses, while the momentum-based formulation is more appropriate when estimating forces, pressure effects, or other momentum-related quantities in the flow. In practice, however, the differences between the two approaches are typically small, as illustrated in the comparison presented in § 3.2.

2.3.2 Flow-region interpretation and limiting behaviour

The GVF form of the effective friction factor, equation (34), can be interpreted in terms of three characteristic streamwise flow regions observed in high-Froude-number aerated flows: a non-aerated clear-water region, a developing aerated flow region, and a downstream quasi-uniform aerated region (figure 1). These regions provide a conceptual framework for understanding how the different terms in the friction factor contribute under varying flow conditions.

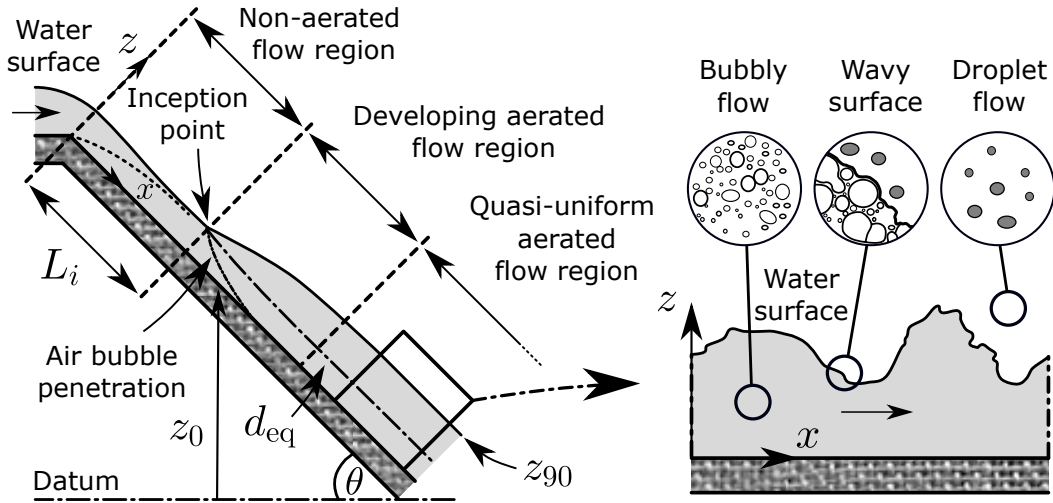


Figure 1: Flow regions and flow structure of an aerated high-Froude-number flow; conceptual sketch expanded from Cain (1978); d_{eq} = equivalent clear-water depth; L_i = upstream distance to aeration inception; x = streamwise coordinate; z = bed-normal coordinate; z_0 = bed elevation relative to datum; z_{90} = mixture flow depth; θ = bed slope angle.

In the non-aerated flow region, air entrainment is absent ($\bar{c} = 0$), and the flow depth equals the equivalent

clear-water depth ($d = d_{\text{eq}} = z_{90}$). The Favre-averaged mixture velocity reduces to the water velocity, $\tilde{u}_m = \overline{u_w}$. Consequently, the momentum correction factor simplifies to its single-phase form

$$\beta = \frac{\int_{z=0}^d \overline{u_w}^2 dz}{d \langle \overline{u_w} \rangle^2},$$

and the pressure correction factor becomes $\Omega = 1$. In this limit, (34) recovers the classical single-phase GVF friction formulation (Hager & Blaser, 1998). For rapidly accelerating flows, boundary-layer-based approaches may be used to estimate the friction factor (Castro-Orgaz & Hager, 2009).

In the developing aerated flow region, the equivalent clear-water depth d_{eq} decreases along the streamwise direction, and the full expression of (34) must be applied. Here, the spatial-development term, proportional to $\Delta d_{\text{eq}}/\Delta x (\beta Fr^2 - \Omega \cos \theta)$, plays a dominant role in determining the effective friction factor.

In the downstream quasi-uniform aerated region, the approximated gradient of the equivalent clear-water depth vanishes ($\Delta d_{\text{eq}}/\Delta x \approx 0$), and (34) attains its limiting form for uniform aerated flow, $f_e = 8gd_{\text{eq}}S_0/\langle \tilde{u}_m \rangle^2 = 8S_0/Fr^2$.

In practice, developing aerated flow is always present downstream of the aeration inception (figure 1), while fully uniform aerated flow occurs only if the chute is sufficiently long. Non-aerated flow exists only upstream of the inception point. The proposed GVF formulation thus provides a practical and physically consistent tool for interpreting and quantifying the spatially varying friction factor across the different flow regions in high-Froude-number aerated flows. For unsteady aerated flows, the temporally varying term from (33) accounts for temporal changes in depth and velocity.

3 Results: Application of the proposed framework

To demonstrate the practical utility of the proposed friction factor framework, we apply the developed GVF formulation to a previous experimental dataset from Bung (2009, $3.9 \leq Fr \leq 6.5$), selectively complementing it with other literature datasets for analyses that do not require detailed velocity measurements. We first present the basic air–water flow parameters and correction factors, which are then used to estimate the streamwise evolution of f_e .

3.1 Air–water flow properties and correction factors

Figure 2 presents representative vertical profiles of the air concentration \bar{c} and the interfacial velocity $\overline{u_{aw}}$. The air concentration profile exhibits a typical S-shaped distribution (figure 2a), whose physical origin has been explained by the two-state convolution approach (Kramer & Valero, 2023; Kramer, 2024). The interfacial velocity $\overline{u_{aw}}$ represents the motion of both water and air immediately adjacent to the interface and is approximately equal to the mixture velocity ($\overline{u_{aw}} \approx \overline{u_m}$), allowing it to be used in depth-averaged momentum calculations. The velocity profile approximately follows a power-law variation through the bulk of the flow, with nearly constant velocity in the upper wavy and spray regions (figure 2b). Both the air concentration and interfacial velocity profiles were measured using a dual-tip phase-detection intrusive probe. Details are provided by Bung (2009).

The momentum correction factor β and the kinetic energy correction factor α for aerated flows arise from Favre averaging and are defined in (11) and (49), respectively, to account for the effects of non-uniform velocity profiles on the mixture momentum and kinetic energy fluxes. Figure 2c presents β and α for the complete dataset of Bung (2009) as functions of the depth-averaged air concentration, defined as

$$\langle \bar{c} \rangle = \frac{1}{z_{90}} \int_{z=0}^{z_{90}} \bar{c} dz. \quad (35)$$

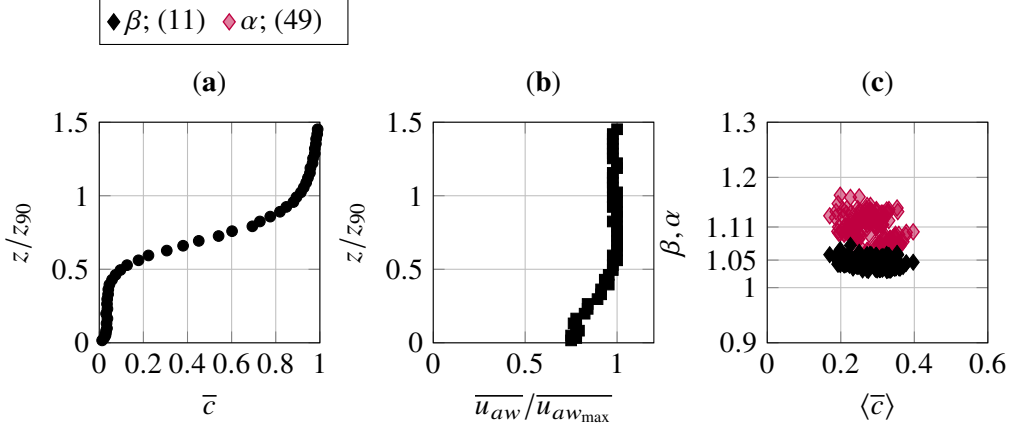


Figure 2: Air–water flow properties, momentum and kinetic energy correction factors for aerated flows (data from Bung (2009)): (a) Representative air concentration profile for $Fr = 4.0$, $q = 0.11 \text{ m}^2/\text{s}$, $\theta = 18.4^\circ$, step height $s = 0.06 \text{ m}$, step edge 11; (b) Corresponding interfacial velocity profile; (c) Momentum correction factors β and kinetic energy correction factors α evaluated for the complete dataset of Bung (2009), with $3.9 \leq Fr \leq 6.5$.

The calculations show that $\beta \approx 1.05$ and $\alpha \approx 1.11$, with a slight decrease for increasing $\langle \bar{c} \rangle$, suggesting that vertical velocity gradients become less pronounced as aeration increases. For comparison, Chanson & Aroquipa Nina (2024) estimated momentum and kinetic energy correction coefficients using an interfacial velocity power-law model and void fraction profiles governed by an advective–diffusion equation. Their results are of the same order of magnitude as those obtained here, supporting the consistency of the present analysis and the validity of the underlying physical assumptions.

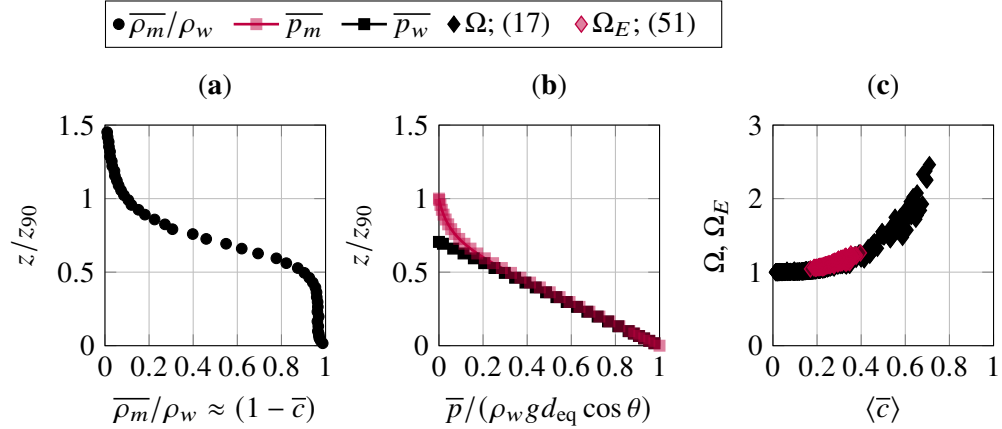


Figure 3: Mixture density profile, pressure distribution, and pressure correction factors Ω and Ω_E for aerated flows: (a) Representative mixture density profile for $Fr = 4.0$, $q = 0.11 \text{ m}^2/\text{s}$, $\theta = 18.4^\circ$, step height $s = 0.06 \text{ m}$, step edge 11 (data from Bung (2009)); (b) Corresponding mixture pressure and clear-water pressure distributions; (c) Pressure correction factors for micro-rough and macro-rough inverts. Ω data from Straub & Anderson (1958), Killen (1968), Bung (2009), Severi (2018), Zhang (2017), and Kramer & Chanson (2018); Ω_E data from Bung (2009).

Figure 3 shows representative density and pressure characteristics of an aerated flow. Panel a presents the mixture density $\bar{\rho}_m(z)$ normalized by the water density ρ_w , while panel b shows the corresponding depth distributions of the mixture pressure (\bar{p}_m) and the equivalent clear-water pressure (\bar{p}_w) . The mixture density

exhibits a mirrored S-shaped profile, directly reflecting the vertical variation of water concentration through the relation $\overline{\rho_m}/\rho_w \approx (1 - \bar{c})$. The mixture pressure $\overline{p_m}$ begins at atmospheric pressure at the mixture depth z_0 , consistent with the standard treatment of aerated flows as a continuous fluid for $0 \leq z \leq z_0$ with depth-varying density (Wood, 1991; Ohtsu *et al.*, 2004; Chanson & Aroquipa Nina, 2024). At the channel bed, the pressure equals $\overline{p_m}(z = 0) = \overline{p_w}(z = 0) = \rho_w g d_{\text{eq}} \cos \theta$, ensuring consistency between the mixture pressure profile and the equivalent depth representation.

Finally, momentum-based pressure correction factors, Ω , as defined in (17), are derived from 571 air concentration profiles for channels with micro- and macro-rough inverts (Straub & Anderson, 1958; Killen, 1968; Bung, 2009; Severi, 2018; Zhang, 2017; Kramer & Chanson, 2018). Energy-based correction factors, Ω_E [equation (51)], are available only for the 179 profiles from Bung (2009, $3.9 \leq Fr \leq 6.5$), since their computation requires detailed velocity measurements. Figure 3c presents the computed pressure correction factors as a function of the depth-averaged air concentration. The results show that the simpler momentum-based factor Ω closely approximates Ω_E , being about 97 % of Ω_E . It also increases with $\langle \bar{c} \rangle$, indicating that the pressure correction factor is largely controlled by the depth-averaged air concentration rather than by bed slope or channel geometry, consistent with Chanson & Aroquipa Nina (2024).

3.2 Streamwise development of effective friction factors

With the momentum correction factor β and the pressure correction factor Ω established, we now estimate f_e -values along the streamwise extent of a gradually varied and statistically steady aerated flow down a stepped chute with $q = 0.11 \text{ m}^2/\text{s}$, $\theta = 18.4^\circ$, step height $s = 0.06 \text{ m}$, and $S_0 = \sin(\theta) = 0.32$, recorded by Bung (2009).

The GVF friction factor formulation (34) requires, in addition to these parameters, knowledge of the Favre-averaged mixture velocity $\langle \tilde{u}_m \rangle$, the Froude number Fr , and the equivalent clear-water depth d_{eq} , along with its approximated streamwise gradient $\Delta d_{\text{eq}}/\Delta x$. For a given flow rate q and equivalent clear-water depth d_{eq} , density-weighting and water-phase continuity imply $\langle \tilde{u}_m \rangle \approx \langle \bar{u}_w \rangle = q/d_{\text{eq}}$. This, in turn, allows the Froude number to be estimated as

$$Fr = \frac{\langle \tilde{u}_m \rangle}{\sqrt{g d_{\text{eq}}}} \approx \frac{q}{\sqrt{g d_{\text{eq}}^3}}. \quad (36)$$

Figure 4a shows the measured streamwise development of the clear-water depth along the aerated region as function of the dimensionless streamwise coordinate $(x - L_i)/d_c$, where L_i denotes the upstream distance to the inception point (figure 1), and $d_c = \sqrt[3]{q^2/g}$ is the critical depth. The data indicate that d_{eq} gradually decreases along the aerated region. Because the measured clear-water depths contain some noise, a smoothing spline was applied to obtain a robust estimate of the depth gradient, shown as the solid black line in figure 4a. Note that the maximum observed gradient was $(\Delta d_{\text{eq}}/\Delta x)_{\text{max}} \approx -2 \times 10^{-3}$.

Using the approximated gradient $\Delta d_{\text{eq}}/\Delta x$, we now evaluate the GVF form of our explicit friction factor expression. Here, we distinguish between the total friction f_e , the uniform flow contribution $f_{e_{\text{uniform}}}$, and the spatial contribution $f_{e_{\text{spatial}}}$

$$f_e = \underbrace{\frac{8 S_0}{Fr^2}}_{f_{e_{\text{uniform}}}} + \underbrace{8 \frac{\Delta d_{\text{eq}}}{\Delta x} \left(\beta - \frac{\Omega \cos \theta}{Fr^2} \right)}_{f_{e_{\text{spatial}}}}. \quad (37)$$

This decomposition allows us to isolate the contributions from uniform and spatially varying components to the total friction factor, as illustrated by the streamwise development in Figure 4b. The spatial term is negative throughout the aerated region because flow depth decreases along the channel ($\Delta d_{\text{eq}}/\Delta x < 0$) as

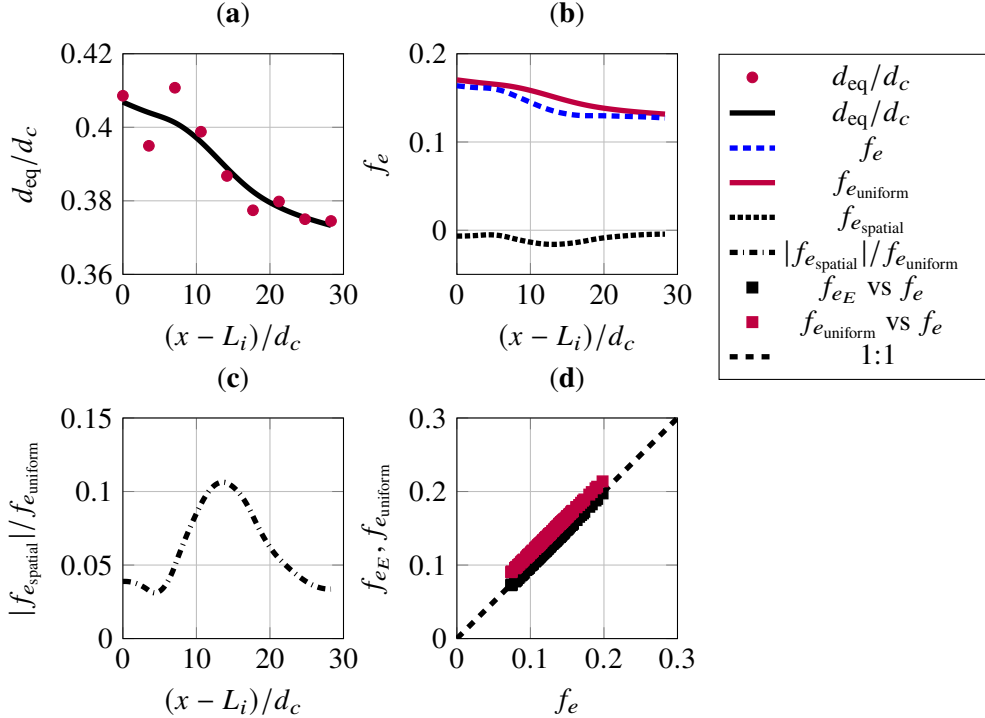


Figure 4: Estimation of effective friction factors in aerated flows: (a) Streamwise development of d_{eq}/d_c for $q = 0.11 \text{ m}^2/\text{s}$, $\theta = 18.4^\circ$, $s = 0.06 \text{ m}$ (data from Bung (2009)); (b) Streamwise decomposition of the total friction factor f_e for the same dataset; (c) Streamwise variation of the ratio between spatial and uniform-flow friction contributions, $|f_{e,\text{spatial}}|/f_{e,\text{uniform}}$, for the same dataset; (d) Comparison of energy-based, momentum-based, and uniform friction factor estimates, with $f_{e,E}$ and $f_{e,\text{uniform}}$ plotted against f_e . The analysis assumes an approximated gradient of $\Delta d_{\text{eq}}/\Delta x \approx -2 \times 10^{-3}$.

the mixture accelerates. This acceleration reduces the effective friction relative to uniform flow, so that $f_e < f_{e,\text{uniform}}$. To quantify this effect, figure 4c shows the ratio $|f_{e,\text{spatial}}|/f_{e,\text{uniform}}$, which reaches a maximum of approximately 0.11, indicating that spatial variation reduces the uniform-flow friction by up to 11 %.

To evaluate differences between the momentum-based and the energy-based friction factor formulation, we calculate f_e [equation (34)] and $f_{e,E}$ [equation (56)] for the full dataset of Bung (2009). The measured depth profiles were noisy, so pointwise derivatives were sometimes unreliable; we therefore assume a representative gradient of $\Delta d_{\text{eq}}/\Delta x \approx -2 \times 10^{-3}$, in accordance with our previous findings. This approximation is sufficient for the purpose of comparing the two formulations. Figure 4d shows the energy-based friction factor $f_{e,E}$ plotted against the momentum based friction factor f_e , revealing very good agreement, with a root-mean-square percentage deviation of 0.88 %. For completeness, the uniform friction factor $f_{e,\text{uniform}}$ is also plotted against f_e , yielding a substantially larger deviation of 14.0 %. Overall, this analysis highlights the importance of accounting for spatial variations when estimating friction factors, while showing that the differences between momentum-based and energy-based formulations are comparatively small.

4 Discussion

4.1 Limitations of the proposed framework

The present work introduces a Favre-averaged Shallow Water Equation (SWE) framework specifically tailored for aerated, high-Froude-number flows. By explicitly accounting for the Favre- and depth-averaged mixture

continuity and momentum, the framework incorporates the effects of air entrainment, non-uniform velocity distributions, and pressure variations within the aerated layer. Building on this SWE foundation, we derive an explicit Darcy–Weisbach friction factor formulation, in which f_e is decomposed into contributions from uniform flow, spatially varying flow, and temporally evolving flow. In addition, an equivalent energy-based GVF formulation is presented in Appendix B, with root-mean-square percentage deviations between the two formulations found to be less than 1% (§ 3.2).

The proposed framework provides a physically consistent means of quantifying friction in aerated flows. Despite these advantages, several limitations and assumptions should be considered:

- **Slowly varying correction factors:** The derivation of (34) assumes that β and Ω vary slowly along the streamwise direction. In flows with abrupt changes in air concentration, or sharp accelerations, this assumption may not hold, and the full friction factor expression (33) should be applied instead.
- **Hydrostatic pressure assumption:** The pressure integration relies on a quasi-hydrostatic approximation, as expressed in (12). This assumption may become less accurate in regions with strongly curved free surfaces, intense turbulence, or significant spray, where dynamic pressure effects are non-negligible.
- **Channel geometry effects:** The friction term is derived using the equivalent clear-water depth d_{eq} . For non-rectangular channels or when sidewall corrections are needed, d_{eq} can be replaced by the hydraulic radius $R_h = A/P$, with the Froude number defined as $Fr = \langle \tilde{u}_m \rangle / \sqrt{g R_h}$, and the spatial gradient term $\Delta d_{eq}/\Delta x$ replaced by $\Delta R_h/\Delta x$. Here, A is the cross-sectional flow area and P is the wetted perimeter. This substitution allows the framework to be applied to trapezoidal or natural channels, although the relationship between spatial derivatives of d_{eq} and R_h may require further calibration for complex geometries.

4.2 Broader impact and applications

The proposed friction factor framework carries several important implications for both fundamental research and engineering practice. First, by providing a systematic and accurate representation of friction in aerated flows, it enables improved predictions of energy dissipation in high-Froude-number spillways, chutes, and open-channel transport systems, which is essential for design, operational planning, and safety assessments.

Second, the explicit formulation is readily applicable to depth-averaged numerical solvers, such as 1D SWE models or CFD approaches, allowing aeration effects to be incorporated through the momentum and pressure correction factors β and Ω without relying on ad hoc tuning parameters. This facilitates more physically consistent simulations of aerated flows across a range of conditions.

Third, the decomposition of the friction factor into uniform, spatially varying, and temporally varying contributions offers enhanced insight into the relative importance of momentum acceleration, hydrostatic pressure gradients, and transient effects in aerated flows. Such mechanistic understanding can help identify the dominant processes in different flow regimes and improve predictive capabilities.

Finally, the framework provides a structured approach for interpreting experimental datasets, identifying conditions where classical uniform-flow formulas fail, and refining empirical or semi-empirical correction factors for both micro-rough and macro-rough invert. This opens avenues for systematic calibration and validation of friction models in aerated flows, bridging the gap between fluid mechanics theory, laboratory experiments, and practical engineering applications.

5 Conclusion

This study presents a physically consistent framework for estimating the effective Darcy–Weisbach friction factor in aerated, high-Froude-number open-channel flows. Starting from the Favre-averaged Shallow Water

Equations for air–water mixtures, we incorporate both momentum and pressure correction factors (β and Ω) to account for non-uniform velocity profiles and aeration-induced modifications of hydrostatic pressure. The resulting formulation explicitly decomposes the friction factor into contributions from uniform flow, spatially varying flow, and temporally varying flow, providing a mechanistic understanding of the relative importance of convective acceleration, pressure gradients, and transient effects.

For gradually varied, steadily developing flows, the framework reduces to a practical expression that can be directly evaluated from measured flow profiles, and for which an energy-based formulation, including kinetic energy and pressure correction factors (α and Ω_E), yields nearly identical results. We apply the framework to an experimental dataset from Bung (2009), demonstrating its ability to capture spatial variations in friction associated with developing aerated flow regions, while recovering classical uniform-flow predictions under quasi-steady downstream conditions. By introducing the hydraulic radius, the formulation can also be extended to non-rectangular channels and more complex geometries.

The proposed framework improves predictions of energy dissipation, informs design and safety assessments in high-Froude-number channels, and provides guidance for both numerical modeling and experimental interpretation. While the model relies on assumptions such as quasi-hydrostatic pressure and slowly varying correction factors, it offers a robust starting point for systematic investigation of aerated flow friction. Moreover, the framework can be directly integrated into 1D SWE solvers, providing a simple yet physically based correction for aeration effects. Future work should focus on detailed pressure measurements and high-resolution depth and velocity profiles to refine the correction factors and extend the framework to more transient and strongly non-uniform flows.

Data Availability Statement. Data, models, and code supporting this study are available from the corresponding author upon reasonable request.

Acknowledgements. Discussions with Dr Hanwen Cui (TMR) and Assoc Prof Stefan Felder (USNW) are acknowledged. Professor Daniel Bung (FH Aachen) is thanked for providing his dataset. The author acknowledges the use of the AI language model ChatGPT (OpenAI) for editorial assistance. All derivations, interpretations, and conclusions in this work are solely those of the author.

Declaration of Interest. The author declares no conflict of interest.

Nomenclature

Latin symbols

A	Cross-sectional flow area (m^2)
c	Volumetric air concentration (–)
d	Single-phase (water) flow depth (m)
d_{eq}	Equivalent clear-water flow depth (m)
e_m	Mechanical energy of the mixture per unit volume ($\text{Pa} = \text{J/m}^3$)
F_e	Local energy flux of the mixture per unit area (W/m^2)
f_e	Equivalent friction factor (–)
Fr	$= \langle \tilde{u}_m \rangle / \sqrt{g d_{\text{eq}}}$; Froude number (–)
g	Gravitational acceleration (m/s^2)

g_x	$= gS_0$; streamwise component of gravitational acceleration (m/s ²)
H_m	Mean total head of the mixture, referenced to the channel bed z_0 (m)
L_i	Upstream distance to aeration inception (m)
P	Wetted perimeter (m)
p	Pressure (N/m ²)
q	Specific water discharge (m ² /s)
R_h	$= A/P$; hydraulic radius (m)
s	Step height (m)
S_0	$= -\partial z_0 / \partial x$ or $\sin \theta$; bed slope (-)
S_f	Friction slope (-)
t	Time (s)
u_m	Streamwise mixture velocity (m/s)
u_w	Streamwise water velocity (m/s)
w_m	Vertical mixture velocity (m/s)
x	Streamwise coordinate measured along the channel bed (m)
z_0	Channel bed elevation, measured vertically from a fixed datum (m)
z	Bed-normal coordinate, measured positive upward from the channel bed (m)
z_{90}	Mixture depth at which $\bar{c} = 0.9$ (m)
$\langle \tilde{z} \rangle$	Favre centroid of the mixture (m)

Greek symbols

α	Kinetic energy correction factor (-)
β	Momentum correction factor (-)
Ω	Momentum-based pressure correction factor (-)
Ω_E	Energy-based pressure correction factor (-)
ρ	Density (kg/m ³)
τ_0	Bed shear stress (N/m ²)
θ	Bed slope angle (rad)
ϕ	Arbitrary quantity (e.g. u_m)
ϕ''	Favre fluctuation of ϕ (same units as ϕ)

Indices and operators

a	Air phase
aw	Air–water interface
GVF	Gradually Varied Flow (steady, spatially developing flow)
max	Maximum
m	Mixture
SWE	Shallow Water Equations
w	Water phase
$\overline{(\cdot)}$	Time-averaging operator; e.g. \overline{u}
$\tilde{(\cdot)}$	Favre (density-weighted) averaging operator; $\tilde{u}_m = \overline{\rho_m u_m} / \overline{\rho_m}$
$\langle \cdot \rangle$	Depth-averaging operator; $\langle \bar{c} \rangle = \frac{1}{z_0} \int_{z=0}^{z_0} \bar{c} dz$
$\langle \tilde{(\cdot)} \rangle$	Favre- and depth-averaging operator; $\langle \tilde{u}_m \rangle = \frac{\int_{z=0}^{z_0} \overline{\rho_m u_m} dz}{\int_{z=0}^{z_0} \overline{\rho_m} dz}$

A Momentum-based friction factor formulation

The density-weighted momentum equation of the Shallow Water Equations (SWE) for aerated flows follows from (31) and is written as

$$\frac{\partial(d_{\text{eq}} \langle \tilde{u}_m \rangle)}{\partial t} + \frac{\partial(\beta d_{\text{eq}} \langle \tilde{u}_m \rangle^2)}{\partial x} = g d_{\text{eq}} S_0 - \frac{\partial}{\partial x} \left(\frac{1}{2} g \Omega d_{\text{eq}}^2 \cos \theta \right) - \frac{\tau_0}{\rho_w}, \quad (38)$$

where d_{eq} is the equivalent clear-water depth, $\langle \tilde{u}_m \rangle$ is the Favre- and depth-averaged water velocity, τ_0 is the bed shear stress, β is the momentum correction factor, and Ω is the pressure correction factor. The bed shear stress is expressed in Darcy-Weisbach form as

$$\tau_0 = \frac{1}{8} \rho_w f_e \langle \tilde{u}_m \rangle^2, \quad (39)$$

which can be substituted into (38), yielding

$$\frac{\partial(d_{\text{eq}} \langle \tilde{u}_m \rangle)}{\partial t} + \frac{\partial(\beta d_{\text{eq}} \langle \tilde{u}_m \rangle^2)}{\partial x} = g d_{\text{eq}} S_0 - \frac{\partial}{\partial x} \left(\frac{1}{2} g \Omega d_{\text{eq}}^2 \cos \theta \right) - \frac{1}{8} f_e \langle \tilde{u}_m \rangle^2. \quad (40)$$

Rearranging for f_e and replacing the derivatives with finite differences gives

$$f_e = \frac{8}{\langle \tilde{u}_m \rangle^2} \left(g d_{\text{eq}} S_0 - \frac{\Delta \left(\frac{1}{2} g \Omega d_{\text{eq}}^2 \cos \theta \right)}{\Delta x} - \frac{\Delta(\beta d_{\text{eq}} \langle \tilde{u}_m \rangle^2)}{\Delta x} - \frac{\Delta(d_{\text{eq}} \langle \tilde{u}_m \rangle)}{\Delta t} \right), \quad (41)$$

which is the most general conservative form of the friction factor expression that directly follows from the SWE momentum equation. It applies to arbitrary unsteady and spatially non-uniform aerated flows, including cases with strong variations in velocity, depth, or aeration. All the parameters in the equation can in principle

be measured or estimated; however, evaluating the derivatives in particular can be cumbersome in practice, especially in highly non-uniform or rapidly varying flows.

To simplify (41) and express it in a Gradually Varied Flow (GVF) framework, we assume steady flow, i.e., $\frac{\Delta(d_{\text{eq}} \langle \tilde{u}_m \rangle)}{\Delta t} \approx 0$. Further, we postulate the β and Ω vary slowly with x , which leads to the following simplifications of the spatial derivatives

$$\frac{\Delta \left(\frac{1}{2} g \Omega d_{\text{eq}}^2 \cos \theta \right)}{\Delta x} \approx g d_{\text{eq}} \frac{\Delta d_{\text{eq}}}{\Delta x} \Omega \cos \theta, \quad (42)$$

$$\frac{\Delta (\beta d_{\text{eq}} \langle \tilde{u}_m \rangle^2)}{\Delta x} \approx \beta \frac{\Delta (d_{\text{eq}} \langle \tilde{u}_m \rangle^2)}{\Delta x} = -\beta g d_{\text{eq}} Fr^2 \frac{\Delta d_{\text{eq}}}{\Delta x}, \quad (43)$$

where the Froude number is defined as $Fr = \langle \tilde{u}_m \rangle / \sqrt{g d_{\text{eq}}}$. The minus sign in (43) arises from applying the steady 1D continuity equation, $d_{\text{eq}} \langle \tilde{u}_m \rangle = q$, which allows us to express the derivative of $d_{\text{eq}} \langle \tilde{u}_m \rangle^2$ in terms of the derivative of d_{eq} . Substituting these expressions into (41) yields a novel expression for the GVF friction factor

$$f_e = \frac{8}{Fr^2} \left(S_0 + \frac{\Delta d_{\text{eq}}}{\Delta x} \left(\beta Fr^2 - \Omega \cos \theta \right) \right) = \underbrace{\frac{8 S_0}{Fr^2}}_{f_{e,\text{uniform}}} + \underbrace{8 \frac{\Delta d_{\text{eq}}}{\Delta x} \left(\beta - \frac{\Omega \cos \theta}{Fr^2} \right)}_{f_{e,\text{spatial}}}. \quad (44)$$

This formulation captures the contributions of convective momentum flux and pressure forces in a steady, gradually varied flow. By assuming slowly varying correction factors, it provides a practical expression for friction in aerated channels while still retaining the effects of non-uniform velocity profiles (β) and aeration-induced pressure correction (Ω). The overall structure of this expression is similar in form to single-phase formulations (e.g., Graf & Song (1995)).

B Energy-based friction factor formulation

We consider an aerated, high-Froude-number flow in a sloping channel with bed slope $S_0 = -\partial z_0 / \partial x$. Let $\tilde{u}_m(z)$ denote the depth-dependent Favre-averaged mixture velocity, where x is aligned with the channel and z is the bed-normal direction (figure 1). Using Favre averaging, the local energy flux of the mixture is written as

$$F_e(z) = \tilde{u}_m e_m(z), \quad (45)$$

where F_e is the energy flux per unit area and $e_m(z)$ is the mechanical energy of the mixture per unit volume. The mechanical energy consists of kinetic, potential, and pressure contributions and is given by

$$e_m(z) = \frac{1}{2} \overline{\rho_m} \tilde{u}_m^2 + \overline{\rho_m} g z \cos \theta + \overline{p_m}, \quad (46)$$

where $\overline{\rho_m}$ and $\overline{p_m}$ are the time-averaged mixture density and pressure, respectively. The former is approximated as $\overline{\rho_m} \approx \rho_w (1 - \bar{c})$, where \bar{c} is the local air concentration and ρ_w is the water density. This approximation neglects air density, which is appropriate for high-speed aerated flows. Integrating the local energy flux over the flow depth yields the total energy flux per unit width, $\int_{z=0}^{z_0} F_e(z) dz$. This integral can be decomposed into kinetic and gravitational (potential plus pressure) components, such that

$$\int_{z=0}^{z_0} F_e(z) dz = \int_{z=0}^{z_0} \frac{1}{2} \overline{\rho_m} \tilde{u}_m^3 dz + \int_{z=0}^{z_0} \tilde{u}_m \overline{\rho_m} g z \cos \theta dz + \int_{z=0}^{z_0} \tilde{u}_m \overline{p_m} dz. \quad (47)$$

The depth-integrated kinetic energy flux can be approximated using the equivalent clear-water depth d_{eq} and the depth-averaged Favre velocity $\langle \tilde{u}_m \rangle$ as

$$\int_{z=0}^{z_0} \frac{1}{2} \overline{\rho_m} \tilde{u}_m^3 dz = \frac{1}{2} \rho_w \int_{z=0}^{z_0} (1 - \bar{c}) \tilde{u}_m^3 dz = \frac{1}{2} \rho_w \alpha d_{\text{eq}} \langle \tilde{u}_m \rangle^3, \quad (48)$$

where the kinetic energy correction factor

$$\alpha = \frac{\langle \tilde{u}_m^3 \rangle}{\langle \tilde{u}_m \rangle^3} = \frac{\int_{z=0}^{z_0} (1 - \bar{c}) \tilde{u}_m^3 dz}{d_{\text{eq}} \langle \tilde{u}_m \rangle^3} \quad (49)$$

accounts for the vertical non-uniformity of the mixture velocity and aeration distribution. The gravitational energy flux includes both potential and pressure contributions. Assuming a hydrostatic pressure distribution based on the local mixture density, the depth-integrated gravitational energy flux can be written as

$$\int_{z=0}^{z_0} \tilde{u}_m (\overline{\rho_m} g z \cos \theta + \overline{p_m}) dz = \rho_w g \cos \theta \Omega_E d_{\text{eq}}^2 \langle \tilde{u}_m \rangle, \quad (50)$$

where the energy-based pressure correction factor

$$\Omega_E = \frac{\int_{z=0}^{z_0} \tilde{u}_m \left((1 - \bar{c}) z + \int_z^{z_0} (1 - \bar{c}(\zeta)) d\zeta \right) dz}{d_{\text{eq}}^2 \langle \tilde{u}_m \rangle} \quad (51)$$

captures the effects of the aeration-induced pressure distribution and the velocity profile. Combining kinetic and gravitational contributions, the total depth-integrated energy flux reads

$$\int_{z=0}^{z_0} F_e(z) dz = \frac{1}{2} \rho_w \alpha d_{\text{eq}} \langle \tilde{u}_m \rangle^3 + \rho_w g \cos \theta \Omega_E d_{\text{eq}}^2 \langle \tilde{u}_m \rangle, \quad (52)$$

which, when normalized by $\rho_w g d_{\text{eq}} \langle \tilde{u}_m \rangle$, defines the flux-averaged total head of the mixture

$$H_m = \frac{1}{\rho_w g d_{\text{eq}} \langle \tilde{u}_m \rangle} \int_{z=0}^{z_0} F_e(z) dz = \alpha \frac{\langle \tilde{u}_m \rangle^2}{2g} + \Omega_E d_{\text{eq}} \cos \theta. \quad (53)$$

Here, the flux-averaged total head H_m is referenced to the channel bed elevation z_0 (figure 1), to maintain consistency with the momentum-based derivation. The friction slope follows from (3)

$$S_f = S_0 - \frac{\partial H_m}{\partial x} = S_0 - \frac{\partial}{\partial x} \left(\alpha \frac{\langle \tilde{u}_m \rangle^2}{2g} + \Omega_E d_{\text{eq}} \cos \theta \right), \quad (54)$$

and the corresponding Darcy–Weisbach friction factor is

$$f_{e_E} = \frac{8g d_{\text{eq}}}{\langle \tilde{u}_m \rangle^2} S_f = \frac{8g d_{\text{eq}}}{\langle \tilde{u}_m \rangle^2} \left(S_0 - \frac{\partial}{\partial x} \left(\alpha \frac{\langle \tilde{u}_m \rangle^2}{2g} + \Omega_E d_{\text{eq}} \cos \theta \right) \right). \quad (55)$$

For gradually varied flows, where streamwise gradients of α and Ω_E are small and 1D continuity holds ($d_{\text{eq}} \langle \tilde{u}_m \rangle = q$), (55) can be simplified

$$f_{e_E} = \frac{8}{Fr^2} \left(S_0 + \frac{\Delta d_{\text{eq}}}{\Delta x} \left(\alpha Fr^2 - \Omega_E \cos \theta \right) \right) = \underbrace{\frac{8 S_0}{Fr^2}}_{f_{e_{\text{uniform}}}} + \underbrace{8 \frac{\Delta d_{\text{eq}}}{\Delta x} \left(\alpha - \frac{\Omega_E \cos \theta}{Fr^2} \right)}_{f_{e_{\text{spatial}}}}, \quad (56)$$

where the derivatives are expressed in finite-difference form, and the local Froude number is $Fr = \langle \tilde{u}_m \rangle / \sqrt{g d_{\text{eq}}}$.

The energy-based friction factor is closely aligned with the corresponding momentum-based formulation. Differences arise naturally from the flux-weighted Favre averaging inherent to the energy balance, since the energy flux contains one additional factor of velocity relative to the momentum flux. As a result, regions of higher velocity contribute disproportionately to the energy flux. These effects are accounted for by the kinetic energy correction factor α and the energy-based pressure correction factor Ω_E . For nearly uniform velocity profiles, $\tilde{u_m} \approx \langle \tilde{u_m} \rangle$, such that $\alpha \approx \beta \approx 1$ and $\Omega_E \approx \Omega$. In this limiting case, the momentum-based and energy-based friction formulations become equivalent.

References

BOES, ROBERT 2000 Two-phase flow and energy dissipation at large cascades (in German). PhD thesis, ETH Zurich, Switzerland, Berkeley, CA.

BOES, R. & HAGER, W. H. 2003 Hydraulic design of stepped spillways. *Journal of Hydraulic Engineering* **129**, 671–679.

BUNG, D. 2009 Zur selbstbelüfteten Gerinnestromung auf Kaskaden mit gemaessigter Neigung. PhD thesis, Bergische Universitaet Wuppertal.

CAIN, P. 1978 Measurements within self-aerated flow on a large spillway. PhD thesis, University of Canterbury, Christchurch, New Zealand.

CASTRO-ORGAS, OSCAR & HAGER, WILLI H. 2009 Hydraulics of developing chute flow. *Journal of Hydraulic Research* **47** (2), 185–194.

CHANSON, H. 1992 Air entrainment in open channel flows: Application to spillways. *La Houille Blanche* (4), 277–286.

CHANSON, H. 1993 Stepped spillway flows and air entrainment. *Canadian Journal of Civil Engineering* **20** (3), 422–435.

CHANSON, HUBERT 1995 *Hydraulic design of stepped cascades, channels, weirs and spillways*. Pergamon, Oxford, U.K.

CHANSON, HUBERT 1997 *Air bubble entrainment in free-surface turbulent shear flows*. Academic Press.

CHANSON, H. 2004 Drag reduction in skimming flow on stepped spillways by aeration. *Journal of Hydraulic Research* **42** (3), 316–322.

CHANSON, HUBERT & AROQUIPA NINA, YVAN 2024 Momentum and energy considerations in self-aerated free-surface flows. *Environmental Fluid Mechanics* **24** (2), 183–202.

FAVRE, A. 1965 Équations des gaz turbulents compressibles: formes générales. *Journal de Mécanique* **4**, 361–390, introduces density-weighted (Favre) averaging for compressible turbulent flows.

FAVRE, A. 1969 Statistical equations of turbulent gases. In *Problems of Hydrodynamics and Continuum Mechanics* (ed. L. I. Sedov), pp. 231–266. Philadelphia: SIAM.

FELDER, STEFAN & CHANSON, HUBERT 2011 Energy dissipation down a stepped spillway with nonuniform step heights. *Journal of Hydraulic Engineering* **137** (11), 1543–1548.

GATSKI, THOMAS B. & BONNET, JEAN-PAUL 2009 *Compressibility, Turbulence and High Speed Flow*. Elsevier.

GRAF, W.H. & SONG, T. 1995 Bed-shear stress in non-uniform and unsteady open-channel flows. *Journal of Hydraulic Research* **33** (5), 699–704.

HAGER, WILLI H. & BLASER, FRANK 1998 Drawdown curve and incipient aeration for chute flow. *Canadian Journal of Civil Engineering* **25** (3), 467–473.

KILLEN, J. M. 1968 The surface characteristics of self aerated flow in steep channels. Phd thesis, University of Minnesota, Minneapolis, MN, USA, 145 pages.

KRAMER, MATTHIAS 2024 Turbulent free-surface in self-aerated flows: superposition of entrapped and entrained air. *Journal of Fluid Mechanics* **980**, A25.

KRAMER, M. & CHANSON, H. 2018 Transition flow regime on stepped spillways: air–water flow characteristics and step-cavity fluctuations. *Environmental Fluid Mechanics* **18**, 947–965.

KRAMER, MATTHIAS & VALERO, DANIEL 2023 Linking turbulent waves and bubble diffusion in self-aerated open-channel flows: two-state air concentration. *Journal of Fluid Mechanics* **966**, A37.

MOZER, ANNE, SELVAM, S. HARISH & SCHÜTTRUMPF, HOLGER 2025 Determining aeration properties over vegetated embankments. *Physics of Fluids* **37** (12), 123331.

OHTSU, I., YASUDA, Y. & TAKAHASHI, M. 2004 Characteristics of skimming flow over stepped spillways. discussion. *Journal of Hydraulic Engineering ASCE* **126** (11), 869–871.

RUFF, J. F. & WARD, P. W. 2002 Hydraulic design of stepped spillways. *Tech. Rep.* U.S. Bureau of Reclamation Denver, Colorado; research project 99FC800156.

SCHERES, B., SCHÜTTRUMPF, H. & FELDER, S. 2020 Flow resistance and energy dissipation in supercritical air-water flows down vegetated chutes. *Water Resources Research* **56** (2).

SEVERI, A. 2018 Aeration performance and flow resistance in high-velocity flows over moderately sloped spillways with micro-rough bed. PhD thesis, School of Civil and Environmental Engineering, UNSW Sydney, Australia.

STRAUB, LORENZ G & ANDERSON, ALVIN G 1958 Experiments on self-aerated flow in open channels. *Journal of the Hydraulics Division* **84** (7), 1–35.

WANG, HANG, BAI, ZHONGTIAN, BAI, RUIDI & LIU, SHANJUN 2022 Self-aeration of supercritical water flow rushing down artificial vegetated stepped chutes. *Water Resources Research* **58** (7).

WILCOX, DAVID C. 1993 *Turbulence Modeling for CFD*. La Cañada, CA: DCW Industries, first edition, 460 pp.

WOOD, I. R. 1991 Free surface air entrainment on spillways. In *Air Entrainment in Free-Surface Flows, IAHR monograph (I.R. Wood ed.)*, A.A.Balkema.

ZHANG, G. 2017 Free-surface aeration, turbulence, and energy dissipation on stepped chutes with triangular steps, chamfered steps, and partially blocked step cavities. Phd thesis, School of Civil Engineering, The University of Queensland, Australia.